GEOFLUIDS

Geofluids (2013) **13**, 56–65 doi: 10.1111/gfl.12010

Weakening processes in thrust faults: insights from the Monte Perdido thrust fault (southern Pyrenees, Spain)

B. LACROIX[1], H. LECLÈRE[2], M. BUATIER[2] AND O. FABBRI[2]

[1]*Institut des Sciences de la Terre, Université de Lausanne, Lausanne, Switzerland;* [2]*UMR Chrono-environnement, Université de Franche Comté, Besancon, France*

ABSTRACT

The Monte Perdido thrust fault (southern Pyrenees) consists of a 6-m-thick interval of intensely deformed clay-bearing rocks. The fault zone is affected by a pervasive pressure solution seam and numerous shear surfaces. Calcite extensional-shear veins are present along the shear surfaces. The angular relationships between the two structures indicate that shear surfaces developed at a high angle (70°) to the local principal maximum stress axis σ_1. Two main stages of deformation are present. The first stage corresponds to the development of calcite shear veins by a combination of shear surface reactivation and extensional mode I rupture. The second stage of deformation corresponds to chlorite precipitation along the previously reactivated shear surfaces. The pore fluid factor λ computed for the two deformation episodes indicates high fluid pressures during the Monte Perdido thrust activity. During the first stage of deformation, the reactivation of the shear surface was facilitated by a suprahydrostatic fluid pressure with a pore fluid factor λ equal to 0.89. For the second stage, the fluid pressure remained still high (with a λ value ranging between 0.77 and 0.84) even with the presence of weak chlorite along the shear surfaces. Furthermore, evidence of hydrostatic fluid pressure during calcite cement precipitation supports that incremental shear surface reactivations are correlated with cyclic fluid pressure fluctuations consistent with a fault-valve model.

Key words: clay minerals, fluid pressure, friction, reactivation, thrust fault

Received 14 June 2012; accepted 13 November 2012

Corresponding author: Brice Lacroix, Institut des Sciences de la Terre, Université de Lausanne, CH-1015 Lausanne, Switzerland.
Email: brice.lacroix@unil.ch. Tel: +41 21 692 4364. Fax: +41 21 692 4305.

Geofluids (2013) **13**, 56–65

INTRODUCTION

In fold-and-thrust belts, shortening is mainly associated with the development of thrust faults. Along such a structure, the displacement can be accommodated by the formation of calcite–quartz shear veins. Numerous studies reveal that these shear veins were formed at a high angle to the greatest principal compressive stress and thus pose a mechanical paradox (i.e., Hubbert & Rubey 1959; Sibson 1985; Fagereng *et al.* 2010; Barker & Cox 2011; Lacroix *et al.* 2011; Buatier *et al.* 2012). Although experiments predict that slip at an angle higher than 30° to σ_1 is not realistic with standard friction coefficient values (Byerlee 1978), slip on faults severely misoriented with respect to σ_1 can occur (e.g., Sibson 1985; Collettini *et al.* 2009a; Leclère *et al.* 2012). To explain the faulting of such faults, different mechanisms lowering the frictional properties of fault zones have been proposed (Collettini *et al.* 2009a). Hubbert & Rubey (1959) proposed that the presence of elevated fluid pressure along the fault zone can allow the reactivation of severely misoriented fault by reducing the normal stress acting on the fault plane. The presence of over-pressurized fluid along the fault zone has been recently revealed by *in situ* measurements along decollement of active offshore accretionary prisms (i.e., Davis *et al.* 1983; Dahlen *et al.* 1984; Dahlen 1990; Moore & Vrolijk 1992). The presence of fluid can also lead to fluid–rock interactions and can trigger the formation of hydrous clay minerals that may facilitate the slip along the fault by lowering slip surface friction. Studies pertaining to faults unfavorably oriented with respect to the remote applied stress have indicated slip weakening in fault cores. Most of these studies concern low-angle normal faults (e.g., Collettini *et al.* 2009a) or strike-slip faults (e.g., Numelin *et al.* 2007), but very few studies investigate thrust faults (Sibson *et al.* 1988 and Fagereng *et al.* (2010) as the only studies).

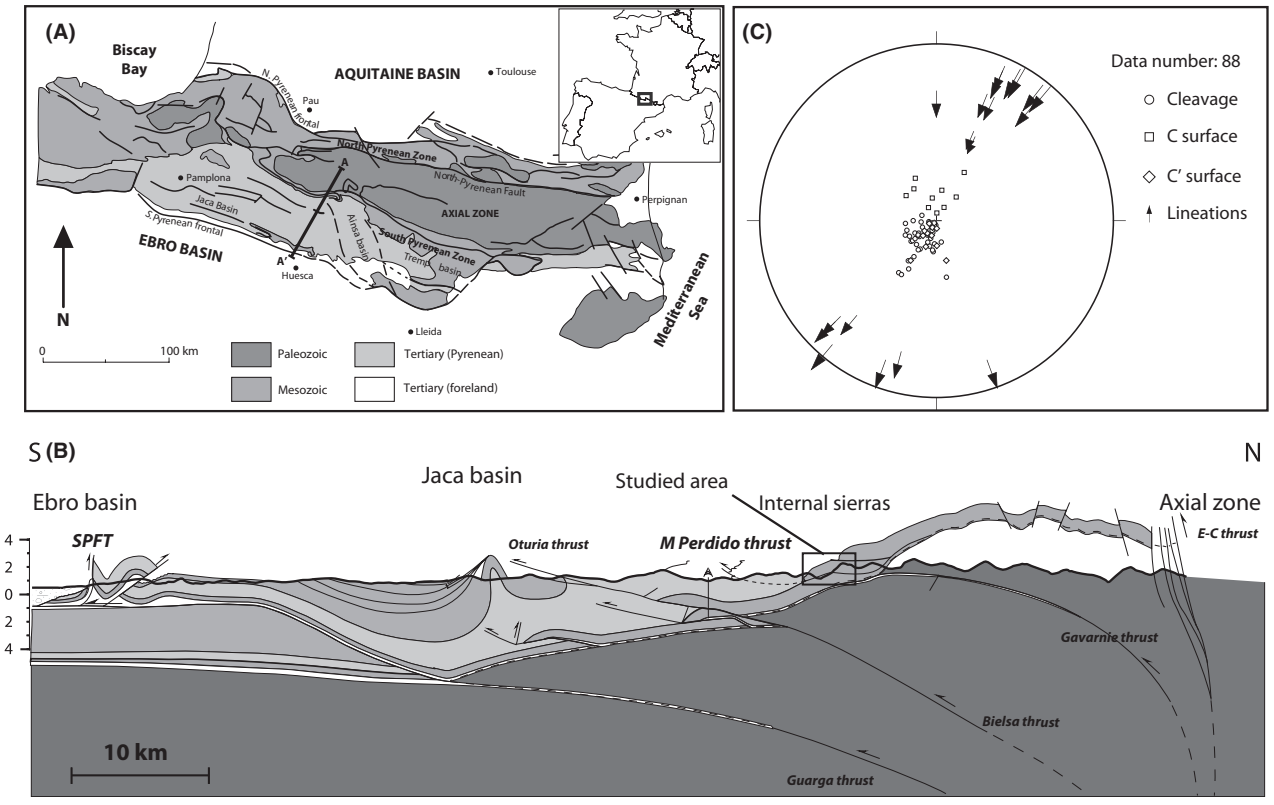

Fig. 1. (A) Structural map of the Pyrenees. (B) Cross-section of the axial zone and South Pyrenean zone (Jaca thrust-sheet-top basin) modified from Meresse (2010) (location: line in A). (C) Schmitd diagram (lower hemisphere) with a plot of cleavage plane poles, shear surfaces, and striations (arrows indicate the sense of displacement of the upper block). All measured structures indicate thrusting toward the S-SW and a near-vertical σ_1.

This article examines the weakening processes of an unfavorably oriented thrust fault in the southern Pyrenees. Structural analyses of the fault were combined with petrographical and scanning electron microscopy (SEM) and transmission electron microscopy (TEM) observations to determine the mechanisms of shear surface reactivation. The contribution of fluid pressure was evaluated using failure mode diagrams in pore fluid factor – differential stress space (Cox 2010).

GEOLOGICAL SETTING

The South Pyrenean Triassic to Oligocene sedimentary basin is affected by southward thrust faults rooted in the Paleozoic basement of the axial zone (Séguret 1972; Fig. 1A). This Eocene to Oligocene fold-and-thrust belt accommodated more than 70% of the total Pyrenean shortening (Teixell 1996). The study focuses on the Monte Perdido thrust fault, the northernmost thrust fault of the South Pyrenean fold-and-thrust belt (Fig. 1B). The horizontal displacement accommodated along the Monte Perdido thrust fault is estimated at 6 km (Séguret 1972). Thrusting of the Monte Perdido sheet occurred during the deposition of the upper part of the Lutetian to Priabonian (47-37 Ma) Hecho Group turbidites (Teixell 1996; Remacha *et al.* 2003). A regional pressure-solution cleavage affected the Monte Perdido thrust unit and is linked to its emplacement (Séguret 1972; Labaume *et al.* 1985; Teixell 1996; Oliva-Urcia *et al.* 2009). The northern part of the Monte Perdido thrust unit was then folded and uplifted by the emplacement of the underlying Gavarnie basement thrust unit during the Priabonian–Rupelian (37-28 Ma) (Séguret 1972; Teixell 1996). The portion of the thrust fault studied here is located at the front of the Monte Perdido thrust unit (Fig. 1B). Consequently, the rotation effect linked to the uplift of the northern axial zone in this fault is negligible. A reactivation of the Monte Perdido thrust fault occurred during activity on the underlying Gavarnie thrust fault (Lacroix *et al.* 2012).

CHARACTERISTICS OF THE MONTE PERDIDO THRUST FAULT

In the studied outcrop, the hanging wall is made up of the Alveolina limestone of the Monte Perdido thrust unit, and the footwall comprises the Hecho Group turbidities of the Gavarnie thrust unit. The fault zone, a 6-m-thick deformed zone, consists of the alternation of several shear surfaces and intensely deformed clay-bearing rocks (Fig. 2A). Pervasive solution cleavages and shear surfaces define C-S-like structures compatible with a south–south-westward dis-

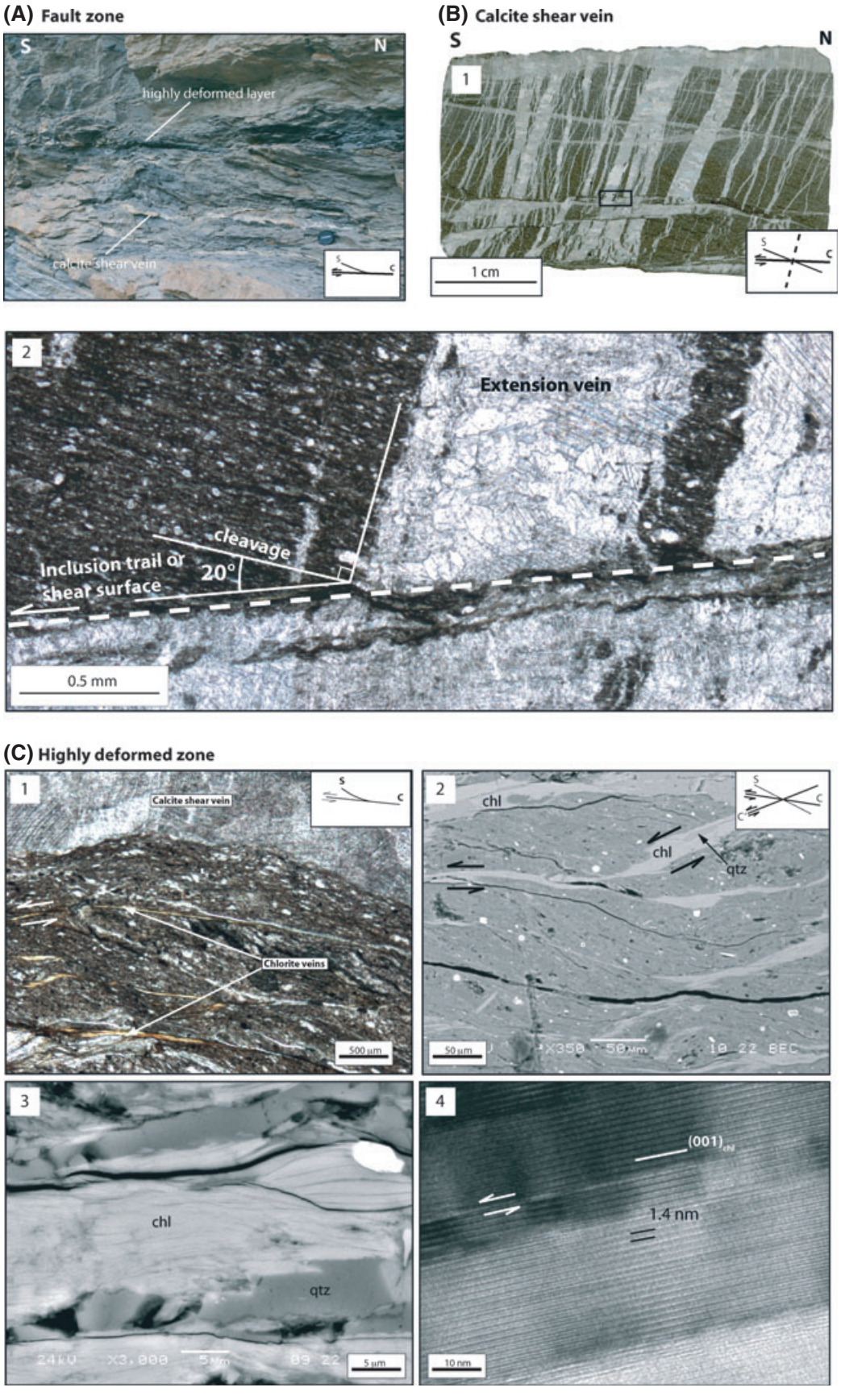
(A) Fault zone
S
N
highly deformed layer
calcite shear vein
(B) Calcite shear vein
S
N
1
1 cm
2
Extension vein
cleavage
20°
Inclusion trail or
shear surface
0.5 mm
(C) Highly deformed zone
1
Calcite shear vein
Chlorite veins
500 µm
2
chl
chl
qtz
50 µm
3
chl
qtz
5 µm
4
(001)chl
1.4 nm
10 nm

Fig. 2. Structures and microstructures observed in the Monte Perdido thrust fault with a top-to-the-south verging. (A) Outcrop of the Monte Perdido thrust fault. Calcite shear veins are present along shear surfaces and define C-S patterns with cleavage surfaces. The highly deformed layer corresponds to a high-strain zone where chlorite is abundant. Note that calcite shear veins and highly deformed layers are parallel. (B) 1. Example of a calcite shear vein composed of a combination of incremental shear surface reactivations and extensional vein openings. 2. Optical microscope image of a calcite shear vein. Note the presence of a cleavage seam at a low angle (20°) to the shear surfaces. Extensional veins crosscut the cleavage at 90°. (C) Optical, scanning electron microscopy (SEM), and TEM observations in a highly foliated zone. 1. Optical view of a high-strain zone. Chlorite precipitated along the reactivated shear surface. Note that shear surfaces with chlorite are parallel to the previous calcite shear vein. 2. SEM image of the high-strain zone with chlorite precipitation along C shear surfaces. 3. Detailed SEM view. Chlorite cement is made up of lamellae comprised between 1 μm and 200 nm in thickness. They are oriented parallel to the shear surfaces, which attests to a crystallization coeval to the shear reactivation. 4. TEM image of chlorite with (001) plane oriented parallel to the shear surface. The 1.4-nm regular spacing between the alternating white and black layers corresponds to the TOTO chlorite (001) layer stacking sequence. The arrows represent the preferential shear displacement along these surfaces with low frictional coefficient and a low intrinsic cohesion. (S: cleavage, C: shear surfaces, chl: chlorite, qtz: quartz).

placement. The angle between the cleavage planes and the shear planes is 20° (Fig 1C). Numerous calcite shear veins are present along the shear surfaces and feature surface lineations with an orientation of N030E. Subvertical extensional veins and subhorizontal pressure solution cleavage as observed along the Monte Perdido thrust fault and in host sediments suggest a near-vertical maximal principal stress axis σ_1 (Fig. 1C). The steeply dipping orientation of the σ_1 axis is in agreement with previous authors showing a subvertical σ_1 axis within thrust fault (Byrne & Fisher 1990; Magee & Zoback 1993; Fagereng 2012). In this study, the angle between gently dipping shear surfaces and steeply dipping σ_1 axis is approximately 70° (Fig. 1C). Locally, highly deformed layers that are darker than other parts of the fault zone correspond to fault reactivation affecting the core zone (Fig. 2A).

According to petrographic, SEM, and TEM observations and to geochemical and thermometric analyses, the Monte Perdido thrust fault underwent two successive deformation episodes. The first stage of deformation is associated with formation of calcite shear veins at temperatures of about 210°C (Lacroix *et al.* 2011; Fig. 2B). The second stage of deformation involved chlorite precipitation along the shear surfaces at temperatures of 240°C during fault reactivation (Fig. 2C; Lacroix *et al.* 2012).

First stage of deformation

In the fault zone, the first stage of deformation is accommodated mainly with incremental slip along shear surfaces and is associated with development of calcite shear veins (Fig. 2A). Similar shear veins, also referred as slickenfibre or bedding parallel veins, have been well documented by Labaume *et al.* (1991), Davison (1995), Lee & Wiltschko (2000), Séjourné *et al.* 2005; and Fagereng *et al.* (2010). Macroscopically, shear veins correspond to centimeter-thick tabular bodies with metric to decametric lateral extent (Fig. 2A). Microscopically, they consist of layered veins opened by a combination of incremental shear surface reactivation and extension vein opening (1 and 2 in Fig. 2B). Each layer corresponds to millimeter-thick sheets bounded by two thin inclusion trails and formed by the lateral succession of numerous millimetric rhomb-shaped tensional veinlets. The inclusion trails correspond to shear surfaces, while the rhomb-shaped veinlets correspond to mode I extensional fractures normal to the cleavage surfaces (1 and 2 in Fig. 2B). Shear surfaces are not sealed by calcite and are assumed to be cohesionless (2 in Fig. 2B). Extension veins subperpendicularly intersect the cleavage (2 in Fig. 2B). When elongated, the calcite fibers are perpendicular to the vein walls and, consequently, are parallel to the cleavage (1 in Fig. 2B). The spatial relationship existing between veins and cleavage seams shows that calcite pressure solution is the major deformation process. Oxygen stable isotope and fluid inclusion analyses demonstrated that calcite veins were formed at a temperature of 210°C (Lacroix *et al.* 2011). Assuming a geothermal paleogradient of 30° C km^{-1}, this temperature corresponds to a burial depth of about 6 km.

Second stage of deformation: chlorite precipitation along shear surfaces

Chlorite is abundant in the highest deformed zones of the Monte Perdido thrust fault where it precipitated along the reactivated C shear surfaces as well as along the inclusion trails within shear veins, to form an interconnected network (1 and 2 in Fig. 2C). The petrographic observations indicate a lack of mode I extension fracture associated with this deformation episode. Consequently, this second stage of deformation is assumed to be strictly frictional and completely accommodated by shearing. As for the first stage of deformation, C shear surfaces have a low angle to the cleavage (20°) (1 and 2 in Fig. 2C). Chlorite precipitates as platelets comprised between 1 μm and 200 nm in thickness (3 in Fig. 2C). They are oriented parallel to shear surfaces, indicating a crystallization coeval to shear reactivation (3 in Fig. 2C). Except for rigid objects such as old calcite veins within which mode I extension fractures are locally observed, this deformation stage is mainly characterized by shear surface reactivation. The presence of authigenic chlorite suggests dissolution recrystallization processes (e.g., Buatier *et al.* 2012). Transmission electron

microscopy images (4 in Fig. 2C) and microprobe analyses confirm the presence of newly formed Fe-chlorite-bearing veins composed of crystals of about 100 nm in thickness with a 1.4 nm regular stacking sequence and with the following structural formula: $(Si_{2.86}Al_{1.14}O_{10}(Al_{1.67}Fe_{2.31}Mg_{1.71})(OH)_8)$. Chlorite crystals display intracrystalline deformation along the (001) plane that could be interpreted as numerous stacking faults in the lattice (4 in Fig. 2C). The P-T conditions during chlorite precipitation are similar to those from stage 1 and are estimated at 240° C and 6.5 km burial depth (Lacroix *et al.* 2012).

REACTIVATION OF THE MONTE PERDIDO THRUST FAULT DURING THE TWO STAGES OF DEFORMATION

According to the results presented above, the Monte Perdido thrust activity is associated with two major deformation events involving the reactivation of the same unfavorably oriented shear surfaces. Following the Mohr–Coulomb failure and assuming a negligible cohesion, the reactivation of the Monte Perdido thrust fault depends on the coefficient of static friction along the reactivated shear surfaces and the pore fluid pressure along the fault zone.

Role of μ_s on fault reactivation

The formation of low-angle calcite shear veins involves simultaneous shear reactivation and extension fracturing under the same stress field between two neighboring shear surfaces (inclusion trails). During the first stage of deformation, the fluid pressure required to create the shear veins has to be high enough to simultaneously (i) allow the formation of extension veins ($\sigma_3' = -T_0$ where T_0 is the tensile strength of the rock and $\sigma_3' = \sigma_3 - P_f$) and (ii) reactivate the cohesionless shear surfaces having a coefficient of static friction of 0.6 and oriented at 70° to the maximum stress σ_1 (Fig. 3A).

The second stage of deformation is characterized by chlorite precipitation along the same misoriented shear surfaces (Fig. 2C). As suggested by the SEM and TEM observations, the (001) chlorite layers are plane-parallel to the shear surfaces (3 and 4 in Fig. 2C). This crystallographic orientation of chlorite crystals provides a preferential sliding surface with low frictional coefficient and a low intrinsic cohesion (Moore & Lockner 2008; Collettini *et al.* 2009b). Recent frictional experiments provide static wet conditions with chlorite friction values varying from 0.26 to 0.4 (Morrow *et al.* 2000; Brown *et al.* 2003; Moore & Lockner 2004; Numelin *et al.* 2007; Collettini 2011; Ikari *et al.* 2011; Behnsen & Faulkner 2012). For this stage of deformation, because of its low frictional strength, the presence of chlorite could have acted as a low-friction mineral favouring stable fault sliding (Moore & Lockner 2004; Behnsen & Faulkner 2012).

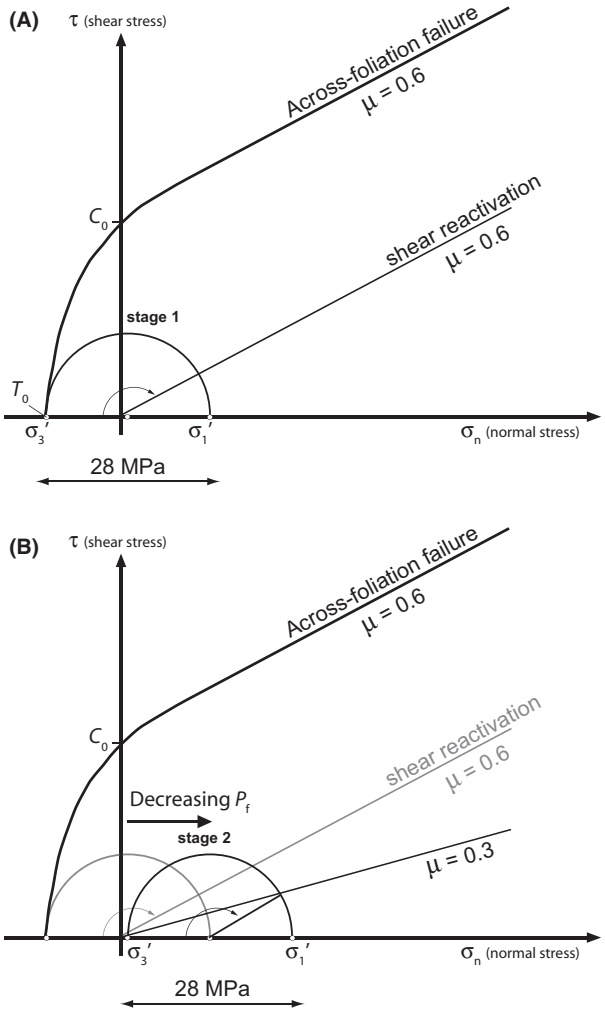

Fig. 3. (A) Mohr diagram (shear stressτ versus effective normal stress σ_n') illustrating conditions of shear vein formation. The conditions for simultaneous shear surface reactivation and extensional fracturing are met when the least principal stress (σ_3') is negative (due to high fluid pressure) and at 70° to the cohesionless fault rock. (B) Mohr diagram illustrating conditions of shear surface reactivation during the second stage of deformation involving chlorite minerals. The lower frictional coefficient of about 0.3 of chlorite minerals allows previous shear surfaces to be reactivated at lower fluid pressure.

Fluid pressure required for the Monte Perdido thrust fault reactivation

The pore fluid factors $\lambda = P_f/\rho_r gz$ required to reactivate the Monte Perdido thrust fault during the two deformation stages were computed using a pore fluid factor–differential stress failure mode diagram proposed by Cox (2010). For an undeformed rock, the failure mode diagram was adopted using the rock density ρ_r fixed at

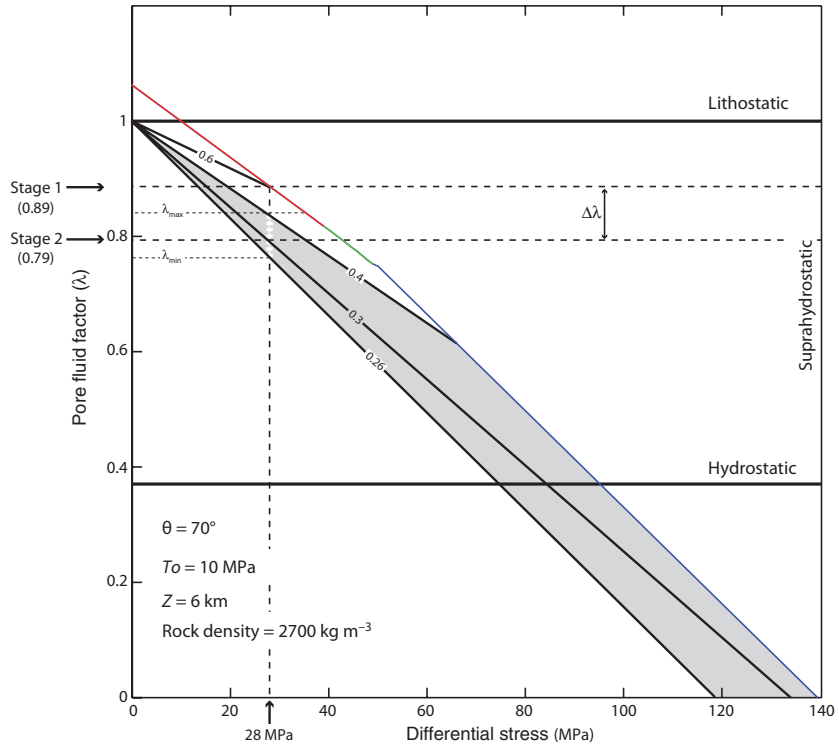

Fig. 4. Pore fluid factor–differential stress diagram showing the pore fluid factor required to reactivate the Monte Perdido thrust fault. The tricolored line represents the failure envelope for an optimal fault with a frictional coefficient of 0.6 and a cohesion of 20 MPa. The shear failure envelope is shown in blue; the extension mode failure is in red; the failure envelope for hybrid extensional-shear mode failure is shown in green. The bold black lines give the pore fluid factor required to reactivate cohesionless shear surfaces oriented at 70° to the maximum stress for a given differential stress and a given pore fluid factor. In this case, the reactivation of shear surfaces during the first stage of deformation is associated with the calcite shear vein development and required a pore fluid factor of approximately 0.9 and a differential stress of about 28 MPa. For the second stage, considering a similar burial depth as proposed by Lacroix *et al.* (2012) and, consequently, assuming a similar differential stress, the computed pore fluid factor varies between 0.77 and 0.84 for a friction coefficient comprised between 0.26 and 0.4 (gray domain). θ: angle to principal stress; T_0: tensile strength; *Z*: depth.

2700 kg m^{-3} (consistent with the bulk mineralogy), the tensile strength T_0 fixed at 10 MPa (consistent with marl and limestone, Karatasios *et al.* 2009), and the cohesive strength C assumed to be 20 MPa (using the relationship $C = 2T$, Cox 2010; Bons *et al.* 2012). The coefficient of static friction of the shear surfaces is fixed, respectively, to 0.6 and 0.3 for the first and second stages of deformation. The reactivated shear surfaces are considered cohesionless. The failure mode diagram was computed with an angle of reactivation of 70° and for a depth of 6 km (Lacroix *et al.* 2011; Fig. 4).

The failure mode diagram shows the brittle failure and reactivation envelopes as a function of the pore fluid factor (λ) and the differential stresses (Fig. 4). The tricolor line corresponds to the failure envelope (for an optimal fault with a frictional coefficient of 0.6 and a cohesion of 20 MPa) separating an upper domain where a new, favorably oriented fault will be formed rather than a reactivated one, from a lower domain where the Monte Perdido thrust fault can be reactivated. The red and green domains, respectively, correspond to extension and extensional-shear hybrid mode failure domains. The blue line corresponds to the shear domains for optimally oriented failure with a coefficient of static friction of 0.6 and a cohesion of 20 MPa. The oblique bold black lines indicate the various pore fluid factors and differential stress required to reactivate the incohesive Monte Perdido thrust fault for different values of static friction μ_s.

During the first deformation stage, the fault reactivation probably occurred in relatively undeformed sediments. As discussed above, this stage of deformation should simultaneously satisfy the reactivation of shear surfaces by sliding and the opening of mode I veins. With μ equal to 0.60, the failure mode diagram predicts that both conditions are satisfied for a differential stress of 28 MPa and a pore fluid factor λ of 0.89 (Fig. 4). Although very low, the calculated differential stress could be realistic as similar low values have been estimated in other thrust faults (e.g., Holl & Anastasio 1995; Ferrill 1998; Lacombe 2001; Fagereng *et al.* 2010). At a 6-km depth, such a pore fluid factor implies a total pore fluid pressure of 145 MPa to

incrementally form calcite shear veins and to reactivate the Monte Perdido thrust fault.

As demonstrated by Lacroix *et al.* (2011), the second stage of deformation occurred at similar burial depths than the first stage of deformation. Consequently, a similar differential stress of 28 MPa can be considered here. For the second stage of deformation, the presence of chlorite (weak mineral) along shear planes has lowered the frictional strength of the fault and favored stable fault sliding (Moore & Lockner 2004; Behnsen & Faulkner 2012). This reduction in frictional strength of the fault implies that the fault could be reactivated with lower fluid pressure than for previous deformation (Fig. 3B). Assuming that during this stage, shear surface slip is dominated by frictional processes rather than pressure-dissolution creep, with a low frictional coefficient of chlorite ranging between 0.26 and 0.4 and a differential stress fixed at 28 MPa, the failure mode diagram predicts an even higher fluid pressure within the suprahydrostatic domain (Fig. 4). More precisely, the pore fluid factor, λ, has a range between 0.77 and 0.84 (Fig. 4). Considering a 6-km depth, the total fluid pressure required to reactivate the Monte Perdido thrust fault must have been between 125 and 136 MPa.

CONTRIBUTION OF WEAKENING PROCESSES IN THE REACTIVATION OF THE MONTE PERDIDO THRUST FAULT

This study suggests that during the first stage of deformation, the formation of calcite shear veins required suprahydrostatic fluid pressure characterized by a pore fluid factor close to 0.9. At 6-km depth, corresponding to the depth of the Monte Perdido thrust activity (Lacroix *et al.* 2011), the pore fluid pressure excess above hydrostatic equilibrium required to reactivate the severely misoriented thrust fault should be about 81 MPa. Such a value is largely above calculated pore fluid pressure excess responsible for the main earthquake and aftershocks in normal seismic faults in the source region of L'Aquila (Terakawa *et al.* 2010). In the case of overthrust faults, high fluid pressure was described as an important parameter lowering the frictional properties of fault zone (Hubbert & Rubey 1959). Furthermore, the pore fluid factor calculated in this study is consistent with actual pore fluid factors measured *in situ* along decollements of active offshore accretionary prisms (i.e., Davis *et al.* 1983; Dahlen *et al.* 1984; Dahlen 1990; Moore & Vrolijk 1992). Based on stable isotope compositions and petrography, Lacroix *et al.* (2011) evidence that deformation inside the Monte Perdido thrust fault is dominated by calcite-diffusive mass transfer of calcite from pressure solution cleavage to shear veins in a relatively closed hydrological system. Such a closed system could create a local permeable barrier facilitating heterogeneous distribution of fluid overpressure and resulting in localized failure of small fault zone patches (Collettini 2002; Mittempergher *et al.* 2011).

During the second stage of deformation, the Monte Perdido thrust fault reactivation was associated with the precipitation of a weak mineral such as chlorite along reactivated shear surfaces that could favors fault creeping. Similar observations have been described in the Zuccale low-angle normal fault in which talc occurred during prograde transformation of dolomite (i.e., Collettini *et al.* 2009a). Moore & Rymer (2007) and Holdsworth *et al.* (2011) proposed that the development of interconnected networks of low-friction clay-bearing surfaces could explain the creeping deformation observed in the San Andreas fault. All these authors suggest that the presence of clay minerals along shear surfaces and with preferential orientation facilitates fault sliding by lowering the internal fault zone frictional coefficient. Although clays are supposed to act as weak minerals able to reduce the pore fluid contribution, the results obtained in this study suggest that fluid pressures still remain high during the second deformation stage even with the formation of a weak mineral such as chlorite. The difference in fluid pressure calculated for the Monte Perdido reactivation between the first and second deformation stages ranges between 9 and 20 MPa depending on the frictional coefficient (Figs 4 and 5).

THRUST FAULT ACTIVITY CYCLE VERSUS FLUID PRESSURE CYCLE

The pore fluid factors calculated in this study clearly show that suprahydrostatic fluid pressure is necessary to reactivate shear surfaces and to form extensional-shear veins (Fig. 4). However, on the basis of a fluid inclusions study, Lacroix *et al.* (2011, 2012) demonstrate that fluid pressure conditions recorded during calcite, quartz, and chlorite precipitations for both deformation stages are purely hydrostatic. This difference in fluid pressure during mineral precipitation and fracture formation suggests that fracture cementation in extensional-shear veins, oriented with a large angle to the principal stress, follows a cyclic fluid pressure between hydrostatic and suprahydrostatic values (Fig. 5). Such fluid pressure cycle has already been proposed by numerous authors (e.g., McCaig 1988; Sibson *et al.* 1988; Boullier & Robert 1992; Robert *et al.* 1995; Wilkinson & Johnston 1996; Parry 1998; among other) and is the basis of the so-called 'fault-valve model' proposed by Sibson *et al.* (1988). However, very few studies have attempted to quantify this effect (i.e., Wilkinson & Johnston 1996 as the only study). Under such fluid pressure fluctuations, fracture formation leads to a decrease in fluid pressure toward hydrostatic values (steps 1 and 3 in Fig. 5). Fluid pressure is known to be an important parameter controlling the mineral solubility (e.g., Renard *et al.*

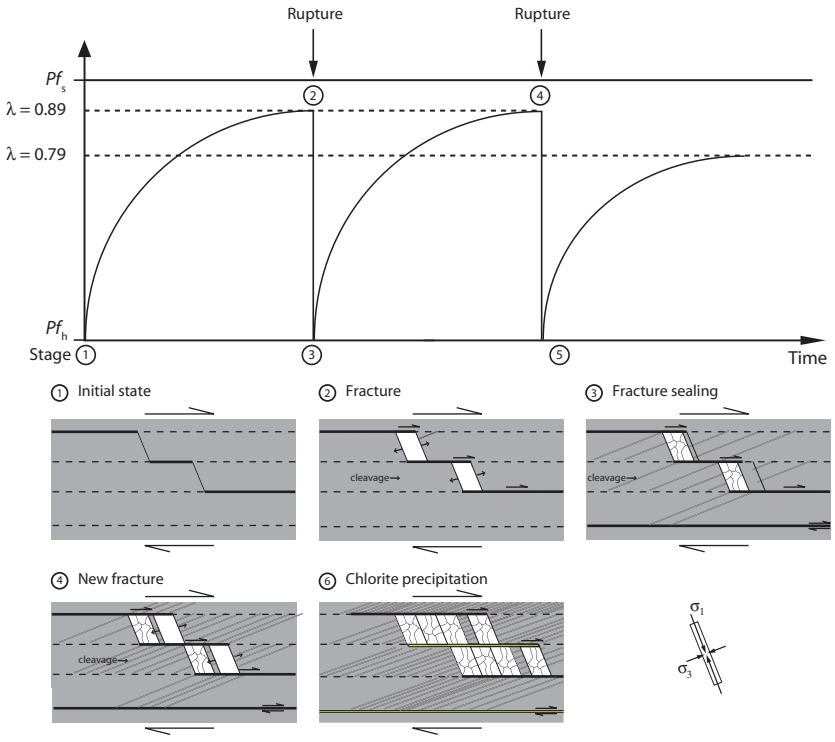

Fig. 5. Graph (not to scale) showing the relation between the fluid pressure cycle (from hydrostatic [Pf_h] to suprahydrostatic [Pf_s]), fracture episodes, and pressure solution processes. Fracture occurs when a high fluid pressure is reached (pore fluid factor of 0.89) and triggers a fluid pressure gradient (1 and 2). Then, calcite pressure solution is activated to seal the fracture (3). Once sealing is accomplished (4), pore pressure increases until the next fracture episode (5). Precipitation of chlorite along shear surfaces during deformation.

2000; Gratier *et al.* 2009). Consequently, such a fluid pressure decrease could be responsible for calcite precipitation along fractures (Sharp 1965; Caciagli & Manning 2003). Considering a low-permeability fault zone, fracturating could be responsible for a local fluid pressure gradient between the fracture and surrounding rocks (patches) and could change the chemical potential driving pressure solution (Gratier *et al.* 2009). This gradient triggers pressure solution in surrounding host rocks where calcite is dissolved along the cleavage and precipitates within fractures (2 and 4 in Fig. 5). Once the fracture is sealed by calcite precipitation, the local fluid pressure increases until the critical value of 145 MPa is attained (λ = 0.9) (Fig. 5) and a new fracture occurs. During the second stage of deformation, although weaker minerals with a preferential crystallographic orientation such as chlorite are present along misoriented shear surfaces, the reactivation of these later requires a pore fluid factor λ of about 0.79 considering a friction coefficient of 0.3 (steps 5 in Fig. 5). The lack of extensive mode I fractures development during this stage compared with the first stage of deformation indicates that the reactivation of shear surfaces did not exceed the hydrofracture criterion as during previous deformation.

Although the absence of seismic textures such as cataclasite and/or fault gouge in the Monte Perdido thrust fault argues for an aseismic slip activity (Gratier & Gamond 1990; Lacroix *et al.* 2011), the present study suggests that at least the first stage of deformation could be related to seismicity. As demonstrated in the previous section, the formation of calcite shear veins is mainly controlled by repeated growth and deformation cycles controlled by periodicity of pore fluid pressure (Fig. 5). Becker *et al.* (2011) propose that episodic opening of veinlets forming crack-seal veins could represent microseismic events. Nevertheless, such seismic activity could be associated with a very low seismic magnitude with negative values (Fagereng 2011). Such seismic behavior is, for example, well demonstrated in the creeping section of the San Andreas fault (e.g., Gratier *et al.* 2011; Mittempergher *et al.* 2011).

CONCLUSIONS

Two different weakening mechanisms occurred along misoriented shear surfaces during the activity of the Monte Perdido thrust fault. During the first stage, shear surfaces were reactivated in rocks with a standard friction (with the friction coefficient varying of 0.6, Byerlee 1978) to form calcite shear veins. This mechanism follows cyclic fluid pressure fluctuations with calcite precipitating at a hydrostatic fluid pressure, whereas suprahydrostatic fluid pressure, with λ = 0.89, is expected to reach the combination of shear reactivation and extension vein opening. In such a system, the low permeability of the fault zone facilitates the increase in fluid pressure responsible for the shear surface reactivation. This process, in which calcite shear veins formed, could be associated with microseismicity.

During the late reactivation episodes, despite the presence of weak chlorite with (001) crystallographic planes

parallel to shear surfaces, fluid pressure still remains high to reactivate the Monte Perdido thrust fault. The differences in total fluid pressure necessary to reactivate shear surfaces between both deformation stages are estimated to range between 9 and 20 MPa.

ACKNOWLEDGEMENTS

This work was realized within the framework of the 3F 'Fault, Fluid, Flow' program funded by INSU-CNRS. We thank S.F. Cox and an anonymous reviewer for constructive comments and Torsten Vennemann for English improvement.

REFERENCES

Barker SLL, Cox SF (2011) Evolution of fluid chemistry and fluid-flow pathways during folding and faulting: an example from Taemas, NSW, Australia. *Geological Society, London, Special Publications*, **359**, 203–27.

Becker S, Hilgers C, Kukla PA, Urai JL (2011) Crack-seal microstructure evolution in bi-mineralic quartz–chlorite veins in shales and siltstones from the RWTH-1 well, Aachen, Germany. *Journal of Structural Geology*, **33**, 676–89.

Behnsen J, Faulkner DR (2012) The effect of mineralogy and effective normal stress on frictional strength of sheet silicates. *Journal of Structural Geology*, **42**, 49–61.

Bons PD, Elburg MA, Gomez-Rivas E (2012) A review of the formation of tectonic veins and their microstructures. *Journal of Structural Geology*, **43**, 33–62.

Boullier AM, Robert F (1992) Palaeoseismic events recorded in Archaean gold-quartz vein networks, Val d'Or, Abitibi, Quebec, Canada. *Journal of Structural Geology*, **14**, 161–79.

Brown KM, Kopf A, Underwood MB, Weinberger JL (2003) Compositional and fluid pressure controls on the state of stress on the Nankai subduction thrust: a weak plate boundary. *Earth and Planetary Science Letters*, **214**, 589.

Buatier MD, Lacroix B, Moutarlier V, Labaume B, Charpentier D, sizun JP, Travé A (2012) Microtextural investigation (SEM and TEM study) of phyllosilicates in a major thrust fault zone (Monte Perdido, southern Pyrenees). Impact on fault reactivation. *Swiss Journal of Geosciences* 105, n°. **2**: 313–24.

Byerlee JD (1978) Friction of rocks. *Pure and Applied Geophysics*, **116**, 615–26.

Byrne T, Fisher D (1990) Evidence for a WEAK and overpressured décollement beneath sediment-dominated accretionary prisms. *Journal of Geophysical Research*, **95**, 9081–97.

Caciagli NC, Manning C (2003) The solubility of calcite in water at 6–16 kbar and 500–800°C. *Contributions to Mineralogy and Petrology*, **146**, 275–85.

Collettini C (2002) Hypothesis for the mechanics and seismic behaviour of low-angle normal faults: the example of the Altotiberina fault Northern Apennines. *Annals of Geophysics*, **45**, 683–98.

Collettini C (2011) The mechanical paradox of low-angle normal faults: current understanding and open questions. *Tectonophysics*, **510**, 253–68.

Collettini C, Niemeijer A, Viti C, Marone C (2009a) Fault zone fabric and fault weakness. *Nature*, **462**, 907–10.

Collettini C, Viti C, Smith SAF, Holdsworth RE (2009b) Development of interconnected talc networks and weakening of continental low-angle normal faults. *Geology*, **37**, 567–70.

Cox SF (2010) The application of failure mode diagrams for exploring the roles of fluid pressure and stress states in controlling styles of fracture-controlled permeability enhancement in faults and shear zones. *Geofluids*, **10**, 217–33.

Dahlen FA (1990) Critical taper model of fold-and-thrust belts and accretionary wedges. *Annual Review of Earth and Planetary Science*, **18**, 55–99.

Dahlen F, Suppe J, Davis D (1984) Mechanics of fold-and-thrust belts and accretionary wedges: cohesive coulomb theory. *Journal of Geophysical Research*, **89**, 10087–101.

Davis D, Suppe J, Dalhen A (1983) Mechanics of fold and thrust-belts and accretionary wedges. *Journal of Geophysical research*, **88**, 1153–72.

Davison I (1995) Fault slip evolution determined from crack-seal veins in pull-aparts and their implications for general slip models. *Journal of Structural Geology*, **17**, 1025–34.

Fagereng A (2011) Frequency-size distribution of competent lenses in a block-in-matrix mélange: imposed length scales of brittle deformation?. *Journal of Geophysical Research*, **116**, B05302.

Fagereng A (2012) On stress and strain in a continuous-discontinuous shear zone undergoing simple shear and volume loss. *Journal of Structural Geology*. In Press.

Fagereng A, Remitti F, Sibson RH (2010) Shear veins observed within anisotropic fabric at high angles to the maximum compressive stress. *Nature Geoscience*, **3**, 482–5.

Ferrill DA (1998) Critical re-evaluation of differential stress estimates from calcite twins in coarse-grained limestone. *Tectonophysics*, **285**, 77–86.

Gratier JP, Gamond JF (1990) Transition between seismic and aseismic deformation in the upper crust. *Geological Society, London, Special Publications*, **54**, 461–73.

Gratier JP, Guiguet R, Renard F, Jenatton L, Bernard D (2009) A pressure solution creep law for quartz from indentation experiments. *Journal Geophysical Research*, **114**, B03403.

Gratier JP, Richard J, Renard F, Mittempergher S, Doan ML, Di Toro G, Hadizadeh J, Boullier AM (2011) Aseismic sliding of active faults by pressure solution creep: evidence from the San Andreas Fault Observatory at Depth. *Geology*, **39**, 1131–4.

Holdsworth RE, van Diggelen EWE, Spiers CJ, de Bresser JHP, Walker RJ, Bowen L (2011) Fault rocks from the SAFOD core samples: implications for weakening at shallow depths along the San Andreas Fault, California. *Journal of Structural Geology*, **33**, 132–44.

Holl JE, Anastasio DJ (1995) Cleavage development within a foreland fold and thrust belt, southern Pyrenees, Spain. *Journal of Structural Geology*, **17**, 357–69.

Hubbert KM, Rubey WW (1959) Role of fluid pressure in mechanics of overthrust faulting. *Geological Society of America Bulletin*, **70**, 115–66.

Ikari MJ, Marone C, Saffer DM (2011) On the relation between fault strength and frictional stability. *Geology*, **39**, 83–6.

Karatasios I, Theoulakis P, Kalagri A, Sapalidis A, Kilikoglou V (2009) Evaluation of consolidation treatments of marly limestones used in archaeological monuments. *Construction and Building Materials*, **23**, 2803–12.

Labaume P, Séguret M, Seyve C (1985) Evolution of a turbiditic foreland basin and analogy with an accretionary prism: example of the Eocene South-Pyrenean Basin. *Tectonics*, **4**, 661–85.

Labaume P, Berty C, Laurent P (1991) Syn-diagenetic evolution of shear structures in superficial nappes: an example from the Northern Apennines (NW Italy). *Journal of Structural Geology*, **13**, 385–98.

Lacombe O (2001) Paleostress magnitudes associated with development of mountain belts: insights from tectonic analyses of calcite twins in the Taiwan Foothills. *Tectonics*, **20**, 834–49.

Lacroix B, Buatier M, Labaume P, Travé A, Dubois M, Charpentier D, Ventalon S, Convert-Gaubier D (2011) Microtectonic and geochemical characterization of thrusting in a foreland basin: example of the South-Pyrenean orogenic wedge (Spain). *Journal of Structural Geology*, **33**, 1359–77.

Lacroix B, Charpentier D, Buatier M, Vennemann T, Labaume P, Adatte T, Travé A, Dubois M (2012) Formation of chlorite during thrust fault reactivation. Record of fluid origin and P–T conditions in the Monte Perdido thrust fault (southern Pyrenees). *Contributions to Mineralogy and Petrology*, **163**, 1083–102.

Leclère H, Fabbri O, Daniel G, Cappa F (2012) Reactivation of a strike-slip fault by fluid overpressuring in the southwestern French-Italian Alps. *Geophysical Journal International*, **189**, 29–37.

Lee YJ, Wiltschko DV (2000) Fault controlled sequential vein dilation: competition between slip and precipitation rates in the Austin Chalk, Texas. *Journal of Structural Geology*, **22**, 1247–60.

Magee ME, Zoback MD (1993) Evidence for a weak interplate thrust fault along the northern Japan subduction zone and implications for the mechanics of thrust faulting and fluid expulsion. *Geology*, **21**, 809–12.

McCaig AM (1988) Deep fluid circulation in fault zones. *Geology*, **16**, 867–70.

Meresse F (2010) Dynamique d'un prisme orogénique intracontinental: evolution thermochronologique (traces de fission sur apatite) et tectonique de la Zone Axiale et des piedmonts des Pyrénées centro-occidentales. Ph.D dissertation. University of Montpellier 2, Montpellier, France.

Mittempergher S, Di Toro G, Gratier JP, Hadizadeh J, Smith SAF, Spiess R (2011) Evidence of transient increases of fluid pressure in SAFOD phase III cores. *Geophysical Research Letter*, **38**, L03301.

Moore DE, Lockner DA (2004) Crystallographic controls on the frictional behavior of dry and water-saturated sheet structure minerals. *Journal of Geophysical Research*, **109**, B03401.

Moore DE, Lockner DA (2008) Talc friction in the temperature range 25°C–400°C: relevance for Fault-Zone Weakening. *Tectonophysics*, **449**, 120–32.

Moore DE, Rymer MJ (2007) Talc-bearing serpentinite and the creeping section of the San Andreas fault. *Nature*, **448**, 795–7.

Moore JC, Vrolijk P (1992) Fluids in accretionary prisms. *Reviews of Geophysics*, **30**, 113–35.

Morrow CA, Moore DE, Lockner DA (2000) The effect of mineral bond strength and adsorbed water on fault gouge frictional strength. *Geophysical Research Letter*, **27**, 815–8.

Numelin T, Marone C, Kirby E (2007) Frictional properties of natural fault gouge from a low-angle normal fault, Panamint Valley, California. *Tectonics*, **26**, TC2004.

Oliva-Urcia B, Larrasoana JC, Pueyo EL, Gil A, Mata P, Parés JM, Schleicher AM, Pueyo O (2009) Disentangling magnetic subfabrics and their link to deformation processes in cleaved sedimentary rocks from the Internal Sierras (west central Pyrenees, Spain). *Journal of Structural Geology*, **31**, 163–76.

Parry WT (1998) Fault-fluid compositions from fluid-inclusion observations and solubilities of fracture-sealing minerals. *Tectonophysics*, **290**, 1–26.

Remacha E, Gual G, Bolaño F, Arcuri M, Oms O, Climent F, Crumeyrolle P, Fernández LP, Vicente JC, Suárez J (2003) Sand-rich turbidite systems of the Hecho Group from slope to the basin plain: facies, stacking patterns, controlling factors and diagnostic features: American Association of Petroleum Geologists, International Conference and Exhibition, Barcelona, Spain, September 21–24. Geological Field Trip no. 12, South-Central Pyrenees.

Renard F, Gratier JP, Jamtveit B (2000) Kinetics of crack-sealing, intergranular pressure solution, and compaction around active faults. *Journal of Structural Geology*, **22**, 1395–407.

Robert F, Boullier AM, Firdaous K (1995) Gold-quartz veins in metamorphic terranes and their bearing on the role of fluids in faulting. *Journal Geophysical Research*, **100**, 12861–79.

Séguret M (1972) Etude tectonique des nappes de séries décollées de la partie centrale du versant sud des Pyrénées. Caractère synsédimentaire, rôle de la compression et de la gravité. Thèse Doct. Publ. USTELA, Série Géologique, Montpellier, 155 pp.

Séjourné S, Malo M, Savard MM, Kirkwood D (2005) Multiple origin and regional significance of bedding parallel veins in a fold and thrust belt: the example of a carbonate slice along the Appalachian structural front. *Tectonophysics*, **407**, 189–209.

Sharp WE (1965) The deposition of hydrothermal quartz and calcite. *Economic Geology*, **60**, 1635–44.

Sibson RH (1985) A note on fault reactivation. *Journal of Structural Geology*, **7**, 751–4.

Sibson RH, Robert F, Poulsen KH (1988) High-angle reverse faults, fluid-pressure cycling, and mesothermal gold-quartz deposits. *Geology*, **16**, 551–5.

Teixell A (1996) The Anso transect of the southern Pyrenees: basement and cover thrust geometries. *Journal of the Geological Society*, **153**, 301–10.

Terakawa T, Zoporowski A, Galvan B, Miller SA (2010) High-pressure fluid at hypocentral depths in the L'Aquila region inferred from earthquake focal mechanisms. *Geology*, **38**, 995–8.

Wilkinson JJ, Johnston JD (1996) Pressure fluctuations, phase separation, and gold precipitation during seismic fracture propagation. *Geology*, **24**, 395–8.

GEOFLUIDS

Volume 13, Number 1, February 2013
ISSN 1468-8115

CONTENTS

WILEY Blackwell

Geofluids* is abstracted/indexed in *Chemical Abstracts

This journal is available online at Wiley Online Library. Visit onlinelibrary.wiley.com to search the articles and register for table of contents and e-mail alerts.